

Effects of Changes in Test Temperature and Loading Conditions on Fracture Toughness of a Zr-Based Bulk Metallic Glass

HALA A. HASSAN, LASZLO KECSKES, and J.J. LEWANDOWSKI

The effects of changes in loading rate and test temperature on the fracture toughness of a Zr-based bulk metallic glass (BMG) were investigated under both displacement-rate-controlled and loading-rate-controlled conditions in three-point bending. The tests were conducted at displacement rates ranging from 0.01 to 10 mm/min, loading rates ranging from 31.5 to 5700 lb/min, and test temperatures from room temperature (298 K) to 623 K. Significant effects of test temperature on the toughness were obtained, while testing under displacement rate control vs loading rate control also produced differences in the toughness and fracture morphology. A preliminary fracture mechanism map is provided to illustrate the effects of changes in temperature and strain rate on the toughness normalized with room-temperature values.

DOI: 10.1007/s11661-008-9549-7

© The Minerals, Metals & Materials Society and ASM International 2008

I. INTRODUCTION

THE interest in metallic glasses has increased after the development of bulk metallic glasses (BMGs) during the early 1990s.^[1,3] Several multicomponent systems such as Zr-Al-Ni,^[2] Zr-Al-Cu-Ni,^[3] and Zr-Ti-Cu-Ni-Be^[1] have been discovered that exhibit exceptional glass formability. Peker and Johnson^[1] reported that Zr-Ti-Cu-Ni-Be forms glass at cooling rates less than 10 K/s, enabling fabrication of fully amorphous rods up to 14 mm in diameter. Some of the BMGs possess strength in excess of structural steel, have greater wear and corrosion^[4] resistance, are tougher than ceramics,^[5,8] and have greater elasticity.

This work is focused on a Zr-Ti-Ni-Cu-Be bulk metallic glass, with tensile strength of 2 GPa^[9,12] and density of 6.1 g/cm³.^[13,14] This BMG is a possible candidate for structural applications because of its high strength-to-weight ratio^[14] and has been used to fabricate golf club heads because of its high strength-to-stiffness ratio.^[14] Recent work has begun to investigate the corrosion resistance,^[5,16] mechanical strength,^[9,11,12,15,17] fatigue behavior,^[18,19] and glass formability^[3] of these materials. Although metallic glasses exhibit almost zero global plastic tensile strain at failure, the elastic strain at failure approaches 2 pct and high local strains are evident on fracture surfaces. Surprisingly high values for toughness have been

reported at room temperature,^[7,8,10] but very little work has been reported on the effects of changes in test temperature up to the glass transition temperature (T_g), or loading conditions, on this property.

The objectives of this work are to determine the effects of changes in test temperature, in addition to changes in loading rate under both displacement rate control and loading rate control on the fracture toughness and the failure mechanisms of a Zr-based BMG. Related recent work has reported the significant effects of displacement rate control vs loading rate control on the tensile properties.^[20]

II. EXPERIMENTAL PROCEDURES

A. Materials

The zirconium-based bulk metallic glass (BMG) used in this investigation is commercially known as Vitreloy I, or Liquidmetal 1 (LM1) (Liquidmetal Technologies, Lake Forest, CA). The composition of this alloy is Zr_{41.8}Ti_{12.9}Cu₁₂Ni_{9.5}Be_{23.8} (at. pct). The general processing details have been summarized elsewhere.^[1] The material was received in the form of plates with 2.7-mm thickness and is identical in composition, including oxygen analyses, to our previous works on this material.^[7,8,11,12,20,22]

B. Specimen Preparation

Fatigue precracks and fracture toughness test experiments were conducted on bend bars in general accordance with ASTM standard E647-2000,^[23] E399-2000,^[24] and E992-1984,^[25] and the British standard BS6835-1.^[26] The toughness standards for J control permit testing under either displacement rate or loading rate control, and both were used in the present tests, as described further subsequently. Electrodischarge

HALA A. HASSAN, formerly Fulbright fellow, CWRU, Cleveland, OH 44106, is now Assistant Professor, with Department of Design and Production Engineering, Faculty of Engineering, Ain Shams University, Cairo, Egypt. LASZLO KECSKES, Research Physical Scientist, is with the US Army Research Laboratory, Aberdeen Proving Ground, MD 21005-5069. J.J. LEWANDOWSKI, Leonard Case, Jr. Professor of Engineering, Department of Materials Science and Engineering, CWRU, Cleveland, OH 44106. Contact e-mail: JLL3@case.edu

Manuscript submitted December 18, 2007.

Article published online May 17, 2008

machining (EDM) was used to cut the BMG to suitable dimensions required for the three-point bending fatigue tests, in general accordance with the standards.^[23,26] General specimen dimensions for the bend bars were in the range of W (width) = 10 mm, B (thickness) = 2.7 mm, and S (span) = 40 mm. The EDM surfaces were first ground through 600 grit in order to remove the EDM layer prior to testing and then polished to a mirror finish to enable crack monitoring and visual examination after testing.

C. Testing Procedure

All tests were carried out on a 50 Kip MTS closed loop servohydraulic machine using a MTS 458...20 controller (MTS, Eden Prairie, MN) and an IBM computer for data acquisition. A starter notch of 200 μ m diameter was placed to a depth of $a/w = 0.2$ to 0.3 using a low-speed Well vertical diamond wire saw. The samples were then fatigue precracked at room temperature to a depth of $a/w = 0.4$ according to the standards^[23,26] to ensure a sharp crack tip in the toughness test. During fatigue precracking, crack growth was measured at a frequency of 20 Hz under decreasing ΔK condition (K control), using an automated load-shedding technique. The load was decreased after every 40 μ m crack growth to provide a decrease in the stress intensity equal to 0.5 MPa \sqrt{m} . The load ratio (R) of 0.1 was used for all fatigue precrack conditions. The crack length during precracking as well as during the toughness testing was measured using the direct current potential drop method (DCPD) and standard formula.^[27]

The subsequent fracture toughness tests were conducted at 298, 505, 603, or 623 K via the use of an Applied Test System (ATS) Inc. temperature-controlled cabinet (ATS Inc., Butler, PA). These temperatures were selected based on the expected softening that will occur near T_g , shown via hot hardness studies,^[28] and from tension tests reported elsewhere.^[29] The DSC measurements of T_g for this material are also reported elsewhere.^[29] The chamber's heating rate was about 0.2 K/s enabling these temperatures to be reached within 1 to

2 hours and controlled within ± 1 K. When the chamber reached the desired temperature, the sample was left to equilibrate for 20 to 25 minutes before running the test, which was monitored and recorded by the LABVIEW program (National Instruments, Austin, TX).

Most of the fracture toughness tests were carried out under displacement rate control, by simply changing the actuator speed over the range 0.01 to 10 mm/min. Some of the tests were conducted under loading rate control, matching the same initial loading rate used in the displacement-rate-controlled tests. In these cases, loading rates of 31.5, 462, and 5722 lb/min were used to provide the same initial displacement rates used in the displacement-rate-controlled tests conducted at 0.05 to 5 mm/min.

III. RESULTS

Table I summarizes each of the test conditions used, while Figure 1 illustrates the range of macroscopic appearance shown by these samples. In addition to test temperature, the effects of different displacement rates ($\dot{\delta}$) and loading rates (\dot{P}) on the toughness are summarized for the displacement-controlled ($\dot{\delta}$) and loading-rate-controlled (\dot{P}) tests, respectively. Also included is the amount of any stable crack growth detected via DCPD, along with the maximum toughness (K_{max}).

A. Displacement-Rate-Controlled Tests

All room-temperature toughness tests exhibited load vs displacement traces that were linear to failure, regardless of loading conditions,^[7,8,11] while higher temperature tests exhibited varying degrees of nonlinearity. Figure 2 schematically shows the effects of changes in the displacement rate on the load vs displacement traces at 505 and 603 K. Significant nonlinearity (R-curve) behavior was obtained at elevated temperatures, as discussed subsequently. The stress intensity, vs change in crack length (Δa) plots for each test are

Table I. Effect of Test Temperature and Loading Conditions on the Fracture Toughness, Fracture Mode, and Amount of Stable Crack Growth: δ = Displacement Rate Control and P = Loading Rate Control

Test Conditions	Fracture Toughness (MPa m ^{1/2})				Fracture Mode		Stable Crack Growth (μ m)	
	$\dot{\delta}$ (mm/min)	\dot{P} (lb/min)	$\dot{\delta}$ Control	\dot{P} Control	$\dot{\delta}$ Control	\dot{P} Control	$\dot{\delta}$ Control	\dot{P} control
298 ^[7,8]	0.1	"	20.5, 19.5, 18.4, 17.8, 17, 17, 15	"	mode I	"	none	"
298 ^[11]	100	"	20	"	mode I	"	none	"
505	0.01	"	80	"	mode I	"	200	"
505	0.05	"	85	"	mode I	"	100	"
603	0.05	31.5	47 (bent)	143	sample bent without fail	shear	none	1000
603	0.5	462	122	85	shear	mode I	350	130
603	5	"	89	"	mode I	"	85	"
623	5	5700	120	98	shear	mode I	280	170
623	10	"	67	"	mode I	"	100	"

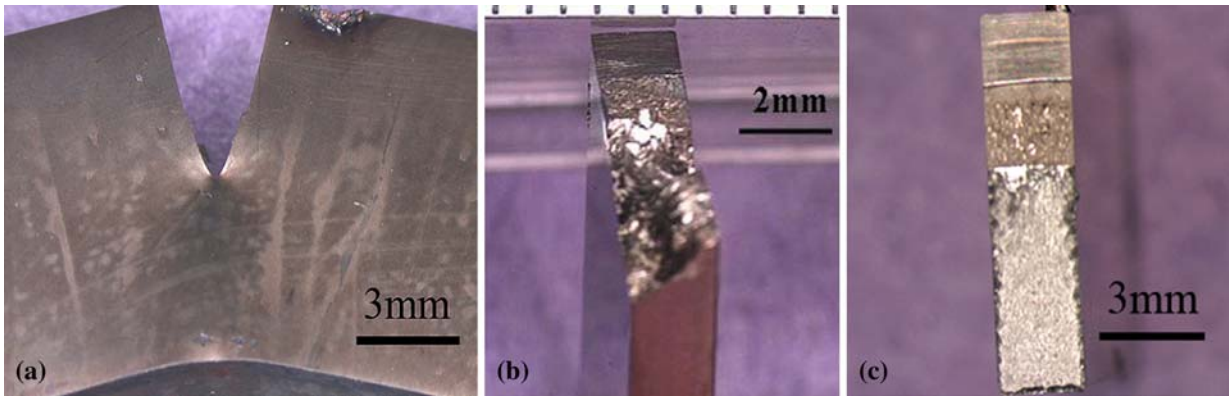


Fig. 1. Macroscopic fracture morphology of Zr-based BMGs tested at different test temperatures and different loading rates. (a) Sample bent without crack growth; $\dot{\delta} = 0.05$ mm/min at $T = 603$ K. (b) Sample failed in shear; $\dot{\delta} = 0.5$ mm/min at $T = 603$ K; $\dot{\delta} = 5$ mm/min and $\dot{P} = 31.5$ lb/min at $T = 623$ K. (c) Sample failed via mode I; $\dot{\delta} = 0.05$ mm/min at $T = 298$ K; $\dot{\delta} = 0.01$ mm/min at $T = 505$ K; $\dot{\delta} = 0.05$ mm/min at $T = 505$ K; $\dot{\delta} = 5$ mm/min at $T = 603$ K; $\dot{\delta} = 10$ mm/min at $T = 623$ K; $\dot{P} = 462$ lb/min at $T = 603$ K; $\dot{P} = 5700$ lb/min at $T = 603$ K.

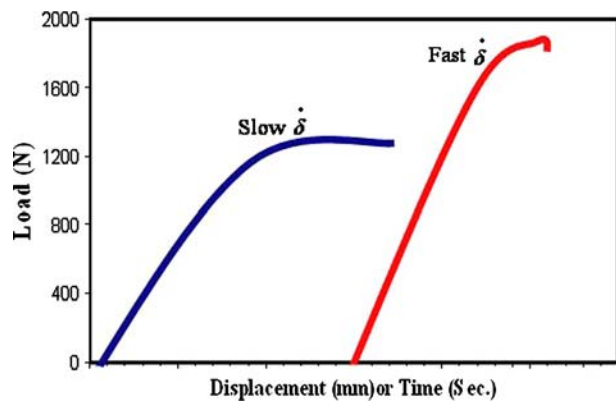


Fig. 2. Schematic showing the effects of different displacement rates on the load-time curves for BMG tested at high temperature (e.g., 505 and 603 K). Slow $\dot{\delta}$ tests ranged from 0.01 to 0.5 mm/min. Fast $\dot{\delta}$ tests ranged from 5 to 10 mm/min.

shown in Figure 3, where DCPD was used to monitor crack length. It was generally observed that increasing the displacement rate (up to a certain value) increased the fracture toughness, while further increases in $\dot{\delta}$ produced reductions in peak load, crack growth, and toughness (Figure 3(a)). The effects of changing the displacement rate on K_{max} at 603 K are shown in Figure 3(a). At the slowest displacement rate ($\dot{\delta}$) used at 603 K, the sample bent with significant crack-tip blunting and without measurable change in the crack length (Figure 1(a)), producing a lower bound $K_Q = 47$ MPa $m^{1/2}$. Increasing the displacement rate $\dot{\delta}$ to 0.5 mm/min produced both an increase in load at fracture and additional crack growth, resulting in K_{max} of 122 MPa $m^{1/2}$, failure via macroscopic shear, and producing the through-thickness slant fracture shown in Figure 1(b). Further increasing $\dot{\delta}$ to 5 mm/min at $T = 603$ K reduced both the peak toughness (i.e., 89 MPa $m^{1/2}$) and the amount of stable

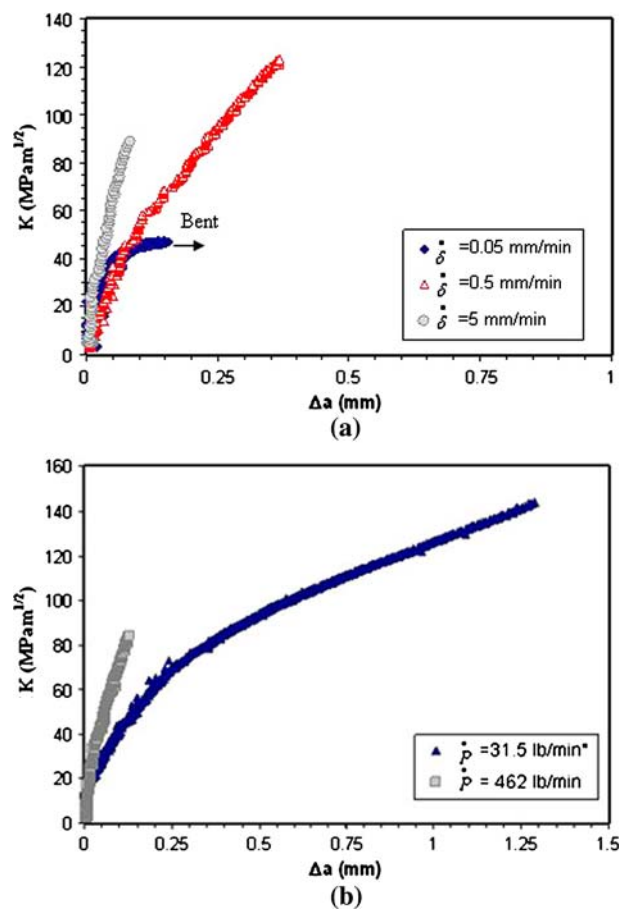


Fig. 3. Stress intensity, K , vs the change in the crack length (Δa) (R curve) for Zr-based BMG precracked at room temperature and tested at $T = 603$ K under different rates for (a) displacement rate control and (b) loading rate control.

crack growth, along with producing mode I failure, as shown in Figure 1(c). Similar results were obtained for displacement-rate-controlled tests conducted at $T = 623$ K, because increasing the displacement rate

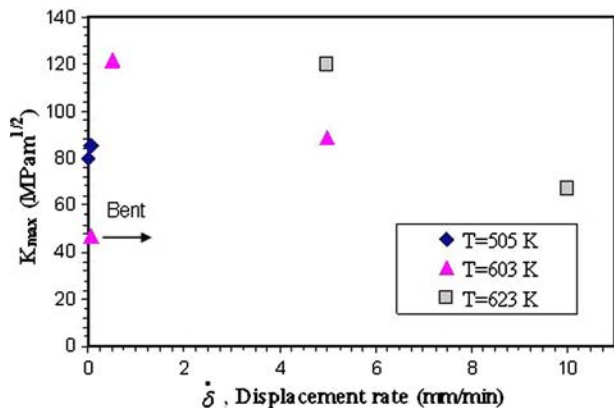


Fig. 4., Effect of changing the displacement rate $\dot{\delta}$ on the fracture toughness of Zr-based BMG at 505, 603, and 623 K.

from 5 to 10 mm/min decreased K_{max} from 120 to 67 MPa $m^{1/2}$, with a reduction in stable crack growth from 280 to 100 μm and a change in fracture morphology from shear (i.e., Figure 1(b)) to mode I failure (i.e., Figure 1(c)). Samples tested under $\dot{\delta} = 0.01$ and 0.05 mm/min at $T = 505$ K showed only a modest increase in the peak toughness K_{max} from 80 to 85 MPa $m^{1/2}$ and mode I failure with a reduction in crack growth from 200 to 100 μm . Figure 4 summarizes the effects of changes in displacement rate on K_{max} for the temperatures tested.

B. Loading-Rate-Controlled Tests

Loading-rate-controlled tests were conducted at 603 K, with loading rates of 462 and 31.5 lb/min conducted to produce the same initial effective displacement rate as the 0.5 and 0.05 mm/min tests conducted under displacement rate control, respectively. The sample tested at $\dot{\delta} = 0.05$ mm/min bent without measurable crack growth, while the loading-rate-controlled test conducted at 31.5 lb/min exhibited stable crack growth at higher loads, thereby producing a much higher toughness of 143 MPa $m^{1/2}$ (Table I and Figure 3(b)) despite the similar initial displacement rate of 0.05 mm/min in both tests. Figure 5 compares the load vs displacement traces for tests conducted at 603 K under displacement rate control of 0.5 mm/min and loading rate control of 462 lb/min. While the initial load vs displacement traces are similar up to 1400 N in Figure 5, significant differences were obtained subsequently. Further increasing the loading rate to 462 lb/min reduced the BMG fracture toughness to 85 MPa $m^{1/2}$, while increasing $\dot{\delta}$ from 0.05 to 0.5 mm/min enabled crack growth at higher load, thereby producing a higher toughness (i.e., 122 MPa $m^{1/2}$) than that obtained at 0.05 mm/min (>47 MPa $m^{1/2}$), which bent and did not fail. Further increasing $\dot{\delta}$ from 0.5 mm/min reduced the toughness and crack growth from 122 MPa $m^{1/2}$ and 350 μm to 89 MPa $m^{1/2}$ and only 85- μm crack growth, respectively.

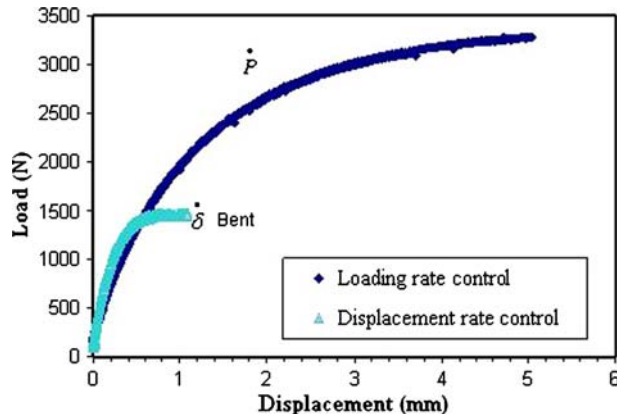


Fig. 5., Difference in load vs displacement traces for tests conducted under loading rate control ($\dot{P} = 462$ lb/min) and displacement rate control ($\dot{\delta} = 0.5$ mm/min) at $T = 603$ K. These tests had the same effective loading rate in the initial loading regime.

C. Effect of Test Temperature

In order to enable comparison of the data, an effective loading rate (ELR) was calculated. The ELR is the amount of load point displacement before yielding (linear part of load vs displacement trace) divided by time.

The effects of changes in test temperature on K_{max} obtained at different ELRs are summarized in Figures 6 and 7. While there is not a significant effect of ELR at very low test temperatures (e.g., $T \leq 505$ K), increasing the test temperature from 603 to 623 K for the samples tested under high loading rate (i.e. 5 mm/min) enhanced K_{max} from 89 to 120 MPa $m^{1/2}$ (Figure 7), while further increases to 10 mm/min reduced the toughness to 67 MPa $m^{1/2}$ (Table II). Increases in test temperature from 505 to 603 K at the same loading rate (e.g., 0.05 mm/min) produced bending in the sample and no measurable crack growth. These results highlight the important combined effects of test temperature and

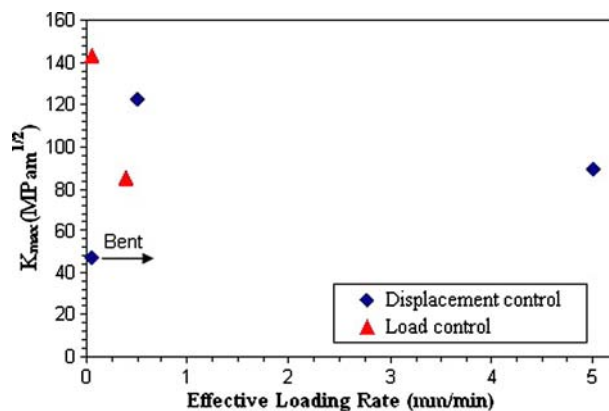


Fig. 6., K_{max} obtained at different effective loading rates under displacement rate control compared to loading rate control for testing conducted at 603 K.

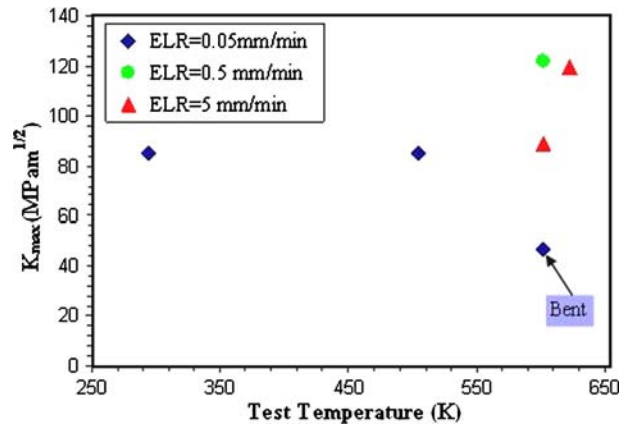


Fig. 7. Effect of test temperature on K_{max} at failure for Zr-based BMG at different temperatures and ELRs.

loading condition on the toughness of BMGs, as discussed subsequently.

IV. DISCUSSION

Previous works^[8,11,30,33] have not revealed a significant effect of changes in loading rate on the fracture toughness of Zr-based glasses at room temperature, although changes in notch radius produce tremendous increases in toughness.^[7,8,11,28] However, the present work shows significant changes in the macroscopic failure mode and toughness of the samples when tested at different temperatures and loading rate conditions, as explained subsequently.

It has been well demonstrated that increasing the test temperature decreases the viscosity of Vit₁,^[24,35] so that it behaves similarly to a viscous liquid where the strength is loading rate and temperature dependent, as shown in recent tension tests on this alloy.^[20] The present work further shows that the toughness and macroscopic fracture mode at high temperature strongly depends on the loading rate (i.e., local strain rate). Wang et al.^[36] established a deformation mechanism map that delineated the boundaries between distinctly different failure modes in tension. They used the following equation to arrive at a critical strain rate in order to produce a change in mechanism from homogeneous to inhomogeneous flow^[37]:

$$\dot{\epsilon} = A \exp\left(\frac{-E_a}{RT}\right) \quad [1]$$

where

A = fitting parameter,
 E_a = activation energy of deformation, and
 R = gas constant (8.314×10^{-3} KJ/mol).

Wang et al.^[36] showed that the differences in flow behavior (i.e., homogeneous vs inhomogeneous) at different strain rates could be rationalized using this approach across a range of temperatures and strain rates. Although the present experiments were conducted on sharply cracked samples, Figure 1 clearly shows a transition in flow/fracture behavior from shear to mode I as the effective loading rate increases, whether this was conducted under displacement rate control or loading rate control. Because of the similarity of observations and realization that flow/fracture in the present pre-cracked experiments are similarly controlled by the temperature and strain-rate-induced changes to the viscosity of the glass, this formula was used to estimate the local strain rate that must be present in order to produce the failure mode obtained for the various testing conditions used presently. In the present case, the homogeneous deformation region is considered for the samples that exhibited the macroscopic sheared fracture surface (i.e., Figure 1(b)). In this regime, the effective strength (i.e., viscosity) of the material must be low enough to create such a large process zone that it approaches the specimen thickness, thereby promoting the through-thickness slant fracture. In contrast, the mode I (i.e., flat) fracture surface represents fracture when the strength (viscosity) of the glasses is higher, because the process zone is well within the thickness of the sample and fracture occurs under nominally plane strain conditions. The calculated strain rate values for some of the testing conditions are shown in Table II, using the correlation provided by Wang.^[36]

Alternately, changing the loading rate (i.e., $\dot{\epsilon}$) also affects the viscosity of the BMG at different temperatures, as shown in previous work^[20,38] on very similar material. Previous work^[38] showed a decrease in the viscosity with increasing $\dot{\epsilon}$ based on the following equation:^[39]

$$\eta/\eta_N = 1 - \exp\left(-\left(\frac{\alpha}{\dot{\epsilon}\eta_N}\right)^\beta\right) \quad [2]$$

Table II. Test Conditions, Failure Mode, and Calculated $\dot{\epsilon}$, η , and σ_Y for the Tested Zr-Based BMG

Sample ID	T (K)	Test Type	Testing Rate	Failure Appearance	K_{max} (MPa m ^{1/2})	$\dot{\epsilon}$ (s ⁻¹)	η (Pa s)	σ (MPa)	E (GPa)
7, 8	298	δ	0.1 mm/min	mode I	18.4 ± 1.4	"	"	2000	100
11	298	δ	100 mm/min	mode I	20	"	"	2000	100
BMGA5-1	603	δ	0.5 mm/min	shear	122	5×10^{-4}	1.5×10^{12}	1425	40
BMGA6-1	603	δ	5 mm/min	mode I	89	2×10^{-2}	3×10^{10}	1800	80
BMGA8-1	603	P	31.5 lb/min	shear	143	1.5×10^{-4}	3×10^{12}	1350	40
BMGA10-1	623	δ	5722 lb/min	mode I	98	6×10^{-2}	1.1×10^{10}	1980	80
BMGA9-1	623	δ	5 mm/min	shear	120	1.5×10^{-3}	3×10^{11}	1350	40
BMGA11-1			10 mm/min	mode I	67	2×10^{-1}	3.3×10^9	2000	85

where

- η = viscosity,
- η_N = Newtonian viscosity, and
- α and β = fitting parameters.

The viscosity for each temperature and strain rate summarized for the present data in Table I was obtained by using the relationship developed in previous work (cf. Figure 8 in Reference 38).

We propose that the change in macroscopic fracture from shear/slant to "at/mode I is related to the size of the plastic zone relative to the sample thickness. In order to determine the plastic zone size at failure, the estimated yield stress of the material was first calculated using the following relationship between the yield stress (σ), viscosity (η), and strain rate ($\dot{\epsilon}$).^[40] Values for $\dot{\epsilon}$ and η were calculated as discussed earlier, while the values for σ were calculated using Eq. 3.^[40]

$$\sigma = 3\eta \cdot \dot{\epsilon} \quad [3]$$

Samples that were tested at high $\dot{\epsilon}$ or \dot{P} failed in "at/mode I manner, and the calculated effective $\dot{\epsilon}$ was relatively high, ranging from $2 \times 10^{-2} \text{ s}^{-1}$ to $2 \times 10^{-1} \text{ s}^{-1}$. The calculated η for these conditions of "at/mode I failure ranged from 3×10^{10} to $3.3 \times 10^9 \text{ Pa s}$,

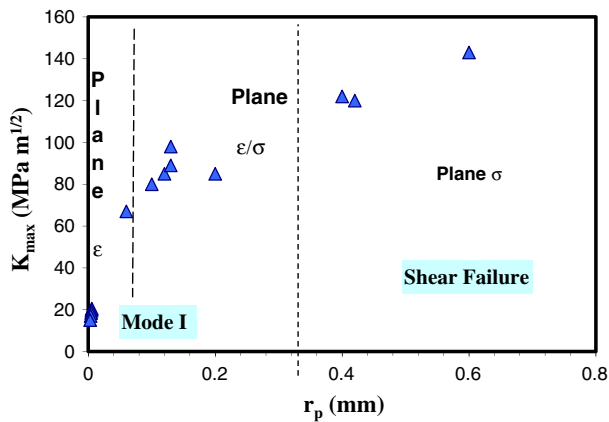


Fig. 8. K_{max} vs calculated plastic zone sizes along with likely stress state present at failure.

respectively. The combined effects of η and $\dot{\epsilon}$ provided the calculated stresses shown in Table I, which are consistent with recently obtained data under both displacement-rate-controlled^[20,38] and loading-rate-controlled^[20] experiments on this material. This information is used in Table III to calculate the plastic zone sizes at K_{max} and the critical thickness for plane strain conditions, using ASTM standards.^[24] The likely stress state (i.e., plane σ , plane ϵ , and mixture plane σ and ϵ) at failure is then presented based on these calculations and compared to the macroscopic failure mode. Table I reveals that samples failing in shear (i.e., Figure 1(b)) consistently exhibited the highest toughness (i.e., K_{max}), while the calculated plastic zone sizes at K_{max} clearly place these samples in plane ϵ . The plastic zone sizes at failure in these samples approach the sample thickness, thereby producing the classic shear mode shown in Figure 1(b), along with the high toughness demonstrated. In contrast, samples tested under nominally plane strain conditions exhibited lower toughness (i.e., K_{max}) and mode I failure, consistent with the smaller plastic zone sizes at failure in these samples. Samples exhibiting a mixture of plane σ and plane ϵ exhibited toughness values intermediate between those in plane σ and plane ϵ , as shown in Table III and summarized in Figure 8; Figure 9 further plots the value of K_{max} against the ratio B/B_{crit} as well as B/r_p , where B is the thickness of the samples tested (i.e., either 2.7 or 4 mm) and B_{crit} and r_p are the critical thickness and plastic zone size for plane strain^[24] given the K_{max} and yield strength of the material, also summarized separately in Table I. Consistent with the information provided in Figure 8, Figure 9 reveals that the test conditions producing high values of K_{max} correspond to samples that have low values of B/r_p and B/B_{crit} , as expected. The lowest values of K_{max} correspond to samples that have high values of B/r_p and B/B_{crit} , consistent with fracture toughness values obtained under plane strain conditions.

The preceding analyses were primarily conducted using the K standards provided by ASTM with regard to the stress states likely present during the test as well as the validity according to the ASTM standards. Because of the large nonlinearity often exhibited and noncatastrophic failure, the results were also analyzed using

Table III. Failure Mode and Calculated r_p , Critical Thickness, and Stress State under Different Test Conditions

ID	Conditions	K_{max} (MPa m ^{1/2})	Plane ϵ r_p (mm)	Plane σ r_p (mm)	B (mm)	B_{crit} (mm)	Stress State	Failure Mode
7, 8	T = 298 K, 0.1 mm/min	18.4 ± 1.4	0.003 to 0.005	0.009 to 0.016	4	0.14 to 0.26	plane ϵ	mode I
11	T = 298 K, 100 mm/min	20	0.005	0.016	4	0.3	plane ϵ	mode I
BMGA1	T = 505 K, 0.05 mm/min	85	0.12	0.36	2.7	5.6	mixed plane ϵ/σ	mode I
BMGA2	T = 505 K, 0.01 mm/min	80	0.10	0.32	2.7	5	mixed plane ϵ/σ	mode I
BMGA4-1	T = 603 K, 0.05 mm/min	47	0.33	1.00	2.7	NA	plane σ	DNF
BMGA5-1	T = 603 K, 0.5 mm/min	122	0.40	1.20	2.7	19	plane σ	shear
BMGA6-1	T = 603 K, 5 mm/min	89	0.13	0.39	2.7	6.2	mixed plane ϵ/σ	mode I
BMGA7-1	T = 603 K, 462 lb/min	85	0.20	0.60	2.7	9.4	mixed plane ϵ/σ	mode I
BMGA8-1	T = 603 K, 31.5 lb/min	143	0.60	1.80	2.7	28	plane σ	shear
BMGA9-1	T = 623 K, 5 mm/min	120	0.42	1.26	2.7	20	plane σ	shear
BMGA10-1	T = 623 K, 5722 lb/min	98	0.13	0.39	2.7	6.7	mixed plane ϵ/σ	mode I
BMGA11-1	T = 623 K, 10 mm/min	67	0.06	0.18	2.7	2.8	plane ϵ	mode I

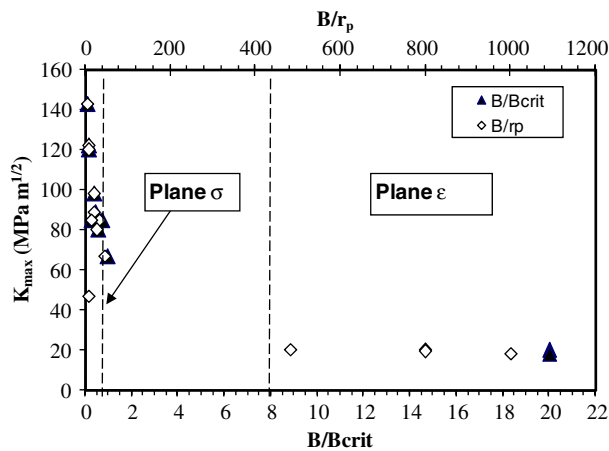


Fig. 9, K_{max} vs B/B_{crit} and K_{max} vs B/r_p along with likely stress state present at failure.

ASTM-E992-84 in terms of the equivalent energy method (i.e., K_{EE}), as well as according to the standards for J testing, ASTM-1820-99.^[41] Table IV summarizes the toughness data according to K_{max} , K_{EE} , and J_{max} . The calculations for K_{max} and K_{EE} both reveal similar trends for the magnitude of toughness under the different test conditions. However, the J-test standard^[41] is more lenient with respect to sample thickness requirements for validity, while Table IV summarizes the J_{max} calculated for the given test conditions. According to the J standard, the following samples exhibit valid data for both the thickness and uncracked ligament criteria: BMGA6-1, BMGA10-1, and BMGA11-1. The following samples exhibit valid data for only the uncracked ligament criteria: BMGA5-1, BMGA8-1, and BMGA9-1. Trends in toughness (i.e., J_{max}) similar to that obtained for K_{max} and K_{EE} were exhibited (Table IV).

The large differences in toughness and failure mode obtained presently when tested under different loading conditions (displacement rate control vs loading rate control) are broadly consistent with recent uniaxial tension data conducted using similar temperature ranges under both displacement rate and loading rate control. In those experiments,^[20] the strength, ductility, and failure mode were strongly affected by such changes in test conditions and rationalized based on the type of flow (e.g., Newtonian and non-Newtonian) likely present in the different test conditions.

That work,^[20] along with previous work,^[38] used the classic Spaepen plot^[42] to rationalize the effects of

changes in test temperature and strain rate on the transition from inhomogeneous flow to homogeneous flow for uniaxial tension^[20] and compression.^[38] The present work also demonstrates the important effects of changes in test temperature, loading rate, and loading conditions (i.e., displacement rate controls loading rate control) on the toughness obtained on fatigue pre-cracked samples for samples of fixed thickness. In the present work, the changes in the loading conditions affect the local strain rate at the crack tip, which thereby affects the flow stress, deformation mechanism, and viscosity of the glass in the crack-tip process zone. The strain rates have been estimated in Table II, while Figure 10 is a schematic fracture mechanism plot of normalized toughness vs normalized test temperature for the samples tested presently at different crack-tip strain rates, somewhat analogous to the deformation mechanism plot originally provided by Spaepen^[42] and more recent attempts to define fracture mechanism maps of crystalline solids.^[43,47] In this regard, Figure 10 is an initial attempt to illustrate the possible effects of changes in crack-tip strain rate on the ratio: fatigue-precracked fracture toughness, K , divided by the room-temperature fracture toughness, K_{RT} , at different temperatures and crack-tip strain rates for a fixed sample thickness. While there are limited data at this time, and much more data are needed over a wider range of strain rates, test temperatures, sample thicknesses, and different metallic glasses, some general observations are clear upon approaching T_g . Fatigue precracked samples tested at sufficiently low strain rates will exhibit homogeneous flow at the crack tip to such an extent that extensive crack-tip blunting and general yielding occurs without any crack growth (Figure 1(a)). Samples tested at somewhat higher strain rates (e.g., 10^{-4} to 10^{-3} s⁻¹) will exhibit through-thickness shear fracture and very high toughness (i.e., region above the solid line) under plane stress conditions due to the large plastic zone size in comparison to the sample thickness (Figures 1(b), 8, and 9). In this regime, increasing the strain rate (e.g., from 10^{-4} to 10^{-3} s⁻¹) decreases the toughness obtained in plane stress due to the change in flow stress and drop in viscosity^[48] at higher strain rates (Table II). Continued increases in the strain rate (e.g., from 10^{-2} to 10^{-1} s⁻¹) continue to decrease the toughness, as shown in Figure 10, and produces a change from shear to mode I failure, as discussed subsequently and shown below the solid line in Figure 10.

Although samples tested at the highest crack-tip strain rates (e.g., 2×10^{-1} s⁻¹) still exhibited toughness

Table IV. Comparison of the Toughness Results Using Different ASTM Standards

ID	Conditions	K_{max} (MPa m ^{1/2})	K_{EE} (MPa m ^{1/2})	J_{max} (KJ/m ²)
BMGA5-1	T = 603 K, 0.5 mm/min	122	125	352
BMGA6-1	T = 603 K, 5 mm/min	89	83.5	140
BMGA7-1	T = 603 K, 462 lb/min	85	80	102
BMGA8-1	T = 603 K, 31.5 lb/min	143	215.8	474
BMGA9-1	T = 623 K, 5 mm/min	120	131	348
BMGA10-1	T = 623 K, 5722 lb/min	98	91.5	146
BMGA11-1	T = 623 K, 10 mm/min	67	64	71

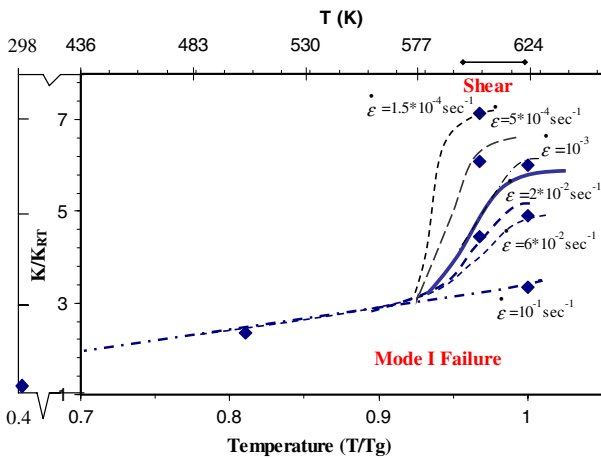


Fig. 10. Preliminary fracture mechanism map for LM-1 tested at 2.7-mm thickness under the conditions shown. Individual data points shown along with transition from higher toughness (shear fracture) to lower toughness mode I fracture. Solid line delineates approximate position of transition.

values well in excess of their room-temperature values, fracture occurred under mode I conditions Figure 1(c). This difference between the high toughness shear fracture (i.e., Figure 1(b)) described previously and that obtained in mode I (i.e. Figure 1(c)) arises due to the significant change in viscosity of the glass and the increase in local flow stress due to the high local strain rate, without a corresponding increase in the local fracture strain. This reduces the plastic zone size at fracture and, hence, the toughness. Decreasing the strain rate in this regime (e.g., from 10^{-1} to 10^{-2} s^{-1}) produces an increase in the toughness with fracture still occurring under mode I conditions (i.e., Figure 1(c)). This apparently arises from the combined effects of the somewhat increased viscosity of the glass and decreased local flow stress (due to the lower strain rate) and increase in the local strain at failure produced by the larger plastic zone size (Table II). Conducting tests at crack-tip strain rates over a wider range of strain rates and temperatures as well as those at much higher strain rates (e.g., $>10^{-1}$ s^{-1}) would be useful in completing this portion of the map in order to investigate the transition in fracture mechanism (i.e., shear vs mode I) and toughness, in addition to determining the limit to toughness at high temperatures in the high-strain-rate regime. Such experiments are planned.

V. CONCLUSIONS

The effects of changes in test temperature and loading rate conditions (i.e., displacement rate controls loading rate control) on the toughness and failure mode of a Zr-based BMG have been determined. Significantly different values for the toughness and failure mode were obtained for samples tested at the same temperature near T_g but different loading conditions (i.e., displacement rate control vs loading rate control). These were rationalized by using recently obtained information on

the effects of changes in test temperature, strain rate, and loading conditions (i.e., displacement rate controls loading rate control) on the flow and fracture of these materials.^[20,38]

Samples tested under conditions of plane strain at room temperature (i.e., significantly below T_g) exhibited the lowest toughness values and were not significantly affected by changes in loading rate over the range examined. Samples tested at elevated temperatures exhibited significant effects of loading conditions (i.e., displacement rate controls loading rate control) as well as changes in loading rate on the magnitude of toughness and extent of stable cracking measured. The significant drop in flow stress and change from intense shear to more homogeneous flow at elevated temperature produced such extensive crack-tip blunting that nR -curve or additional cracking was measured at the slowest displacement rate at 603 K. However, increases to the displacement rate or loading rate produced changes to the viscosity of the glass and increased the flow stress of the material in the crack-tip region to such an extent that fracture and R-curve behavior at elevated toughness were often observed. The magnitude of toughness and extent of stable crack growth were affected by test temperature as well as loading conditions (i.e., displacement rate control vs loading rate control) and loading/displacement rate. Transition from higher toughness through-thickness shear fracture to mode I failure at reduced toughness occurred upon increasing the strain rate sufficiently. A normalized plot of toughness vs test temperature was constructed in order to delineate the different fracture regimes exhibited.

ACKNOWLEDGMENTS

The authors express great appreciation to Liquid-metal Technologies and the Army Research Labs for the supply of materials as well as Grant Nos. ARO-DAAD19-02-1-0364 and ONR-N00014-03-1-0205 for financial support. The technical support of Chris Tuma in providing mechanical testing system instructions and solutions is much appreciated as are the discussions and experimental support from Alan Vormelker and Dr. R. Varadarajan. One of the authors (HAH) acknowledges the support of the U.S.-Egypt Joint Board on Scientific and Technological Cooperation for the Junior Scientist Development Visit Grant 2005/2006 to conduct this work. She also acknowledges The Fulbright Association for her current Fulbright Scholar position at CWRU for 2006/2007. The authors thank the anonymous reviewer that suggested the construction of the initial fracture mechanism map (Figure 10).

TABLE OF SYMBOLS

•	displacement control rate (mm/min)
δ	
\dot{P}	load control rate (lb/min)
η	viscosity (Pa s)

η_N	Newtonian viscosity
$\dot{\epsilon}$	strain rate (s^{-1})
ELR	effective loading rate (mm/min)
T_g	glass transition temperature (K)

REFERENCES

1. A. Peker and W.L. Johnson: *Appl. Phys. Lett.*, 1993, vol. 63, pp. 2342...44.
2. A. Inoue, T. Zhang, and T. Masumoto: *Mater. Trans. JIM*, 1990, vol. 31 (5), pp. 177...83.
3. T. Zhang, A. Inoue, and T. Masumoto: *Mater. Trans. JIM*, 1991, vol. 32, pp. 1005...10.
4. S.J. Pang, T. Zhang, K. Asami, and A. Inoue: *Acta Mater.*, 2002, vol. 50, pp. 489...97.
5. A. Gebert, U.K. Mudali, J. Eckert, and L. Schultz: *Mater. Res. Soc. Symp. Proc.*, 2004, vol. 806, p. 369.
6. A. Leonhard, L.Q. Xing, M. Heilmaier, A. Gebert, J. Eckert, and L. Schultz: *Nanostruct. Mater.*, 1998, vol. 10, pp. 805...14.
7. P. Lowhaphandu and J.J. Lewandowski: *Scripta Mater.*, 1998, vol. 38, pp. 1811...17.
8. P. Lowhaphandu, L.A. Ludrosky, S.L. Montgomery, and J.J. Lewandowski: *Intermetallics*, 2000, vol. 8, pp. 487...92.
9. H.A. Bruck, T. Christman, A.J. Rosakis, and W.L. Johnson: *Scripta Mater.*, 1994, vol. 30, pp. 429...34.
10. C.J. Gilbert, R.O. Ritchie, and W.L. Johnson: *Appl. Phys. Lett.*, 1997, vol. 71, pp. 476...79.
11. J.J. Lewandowski: *Mater. Trans. JIM*, 2001, vol. 42(4), pp. 633...37.
12. J.J. Lewandowski and P. Lowhaphandu: *Phil. Mag. A*, 2002, vol. 82 (17), pp. 3427...41.
13. C.C. Aydiner, E. Ustundag, M.B. Prime, and A. Peker: *J. Non-Crystalline Solids*, 2003, vol. 316, pp. 82...95.
14. M. Telford: *Mater. Today*, 2004, Mar., pp. 36...43.
15. R. Schennach, T. Grady, D.G. Naugle, H. McWhiney, C.C. Hays, W.L. Johnson, and D.L. Cocke: *J. Vac. Sci. Technol. A*, 2001, vol. 19 (4), part I, pp. 1447...53.
16. J.R. Scully, A. Gebert, and J.H. Payer: *J. Mater. Res.*, 2007, vol. 22 (2), pp. 302...13.
17. A.L. Greer: *Science*, 1995, vol. 267, pp. 1947...53.
18. H.A. Davies: in *Amorphous Metallic Alloys*, F.E. Luborsky, ed., Butterworth and Company, London, 1983, p. 8.
19. G.Y. Wang, P.K. Liaw, A. Peker, B. Wang, M.L. Benson, w. Yuan, W.H. Peter, L. Huang, M. Freels, R.A. Buchanan, C.T. Liu, and C.R. Brooks, *Mat. Res. Soc. Symp. Proc. "Amorphous and Nanocrystalline Metals"*, R. Busch, T.C. Hufnagel, J. Eckert, A. Inoue, W.J. Johnson, and A.R. Yavari, eds., 2004, vol. 806, pp. 331...41.
20. A. Vormelker, L.O. Vatamanu, L. Kecskes, and J.J. Lewandowski: *Metall. Mater. Trans. A*, 2008, vol. 39A, DOI [10.1007/s11661-007-9410-4](https://doi.org/10.1007/s11661-007-9410-4) in press.
21. G. Sunny, J.J. Lewandowski, and V. Prakash: *J. Mater. Res.*, 2007, vol. 22(2), pp. 389...401.
22. F. Yuan, J.J. Lewandowski, and V. Prakash: *J. Mater. Res.*, 2007, vol. 22 (2), pp. 402...11.
23. Standard Test Method for Measurement of Fatigue Crack Growth Rates, ASTM E647-98, ASTM, Philadelphia, PA, 2000.
24. Standard Test Method for Plane Strain Fracture Toughness of Metallic Materials, ASTM E399-2000, ASTM, Philadelphia, PA, 2000.
25. Standard Practice for Determination of Fracture Toughness of Steels Using Equivalent Energy Method, ASTM E992-1984, ASTM, Philadelphia, PA, 1984.
26. British Standard Method for Determination of the Rate of Fatigue Crack Growth in Metallic Materials, BS 6835-SEN B3, British Standard Institution, London, UK, 1988.
27. H.H. Johnson: *Mater. Res. Stand.*, 1965, vol. 5(9), pp. 442...45.
28. J.J. Lewandowski, M. Shazly, and A. Shamimi Nuori: *Scripta Mater.*, 2006, vol. 54(3), pp. 337...41.
29. W.L. Johnson: *Prog. Mater. Sci.*, 1986, vol. 30, pp. 81...134.
30. P. Wesseling, P. Lowhaphandu, and J.J. Lewandowski: *Mater. Res. Soc. Symp. Proc.*, 2003, vol. 754, p. 281.
31. K. Fujita, A. Okamoto, N. Nishiyama, Y. Yokoyama, H. Kimura, and A. Inoue: *J. Alloys Compd.*, 2007, vols. 434...435, pp. 22...27.
32. K. Fujita, N. Nishiyama, K. Amiya, T. Zhang, H. Kimura, and A. Inoue: *J. Metastable Nanocryst. Mater.*, 2005, vols. 24...25, pp. 323...26.
33. A. Kawashima, H. Kurishita, H. Kimura, T. Zhang, and A. Inoue: *Mater. Trans.*, 2005, vol. 46(7), pp. 1725...32.
34. A. Masuhr, R. Busch, and W.L. Johnson: *J. Non-Cryst Solids*, 1999, part 2, pp. 566...71.
35. A. Masuhr, T.A. Waniuk, R. Busch, and W.L. Johnson: *Phys. Rev. Lett.*, 1999, vol. 82, pp. 2290...93.
36. G. Wang, J. Shen, J.F. Sun, Z.P. Lu, Z.H. Stachurski, and B.D. Zhou: *Intermetallics*, 2005, vol. 13, pp. 642...48.
37. Y. Kawamura, T. Shibata, A. Inoue, and T. Masumoto: *Mater. Trans. JIM*, 1999, vol. 40(4), pp. 794...803.
38. J. Lu, G. Ravichandran, and W.L. Johnson: *Acta Mater.*, 2003, vol. 51, pp. 3429...43.
39. S. Matsuka: *Relaxation Phenomena in Polymers*, Hanser Publishers, New York, NY, 1992.
40. F.T. Trouton: *Proc. R. Soc., London*, 1906, vol. 77, pp. 426...40.
41. Standard Test Method for Measurement of Fracture Toughness, ASTM E1820-99, ASTM, Philadelphia, PA, 1999.
42. F. Spaepen: *Acta Metall.*, 1977, vol. 25, pp. 407...15.
43. P.J. Wray: *J. Appl. Phys.*, 1969, vol. 40, pp. 4018...29.
44. M.F. Ashby: Cambridge University Engineering Department Report No. CUED/C/MATS/TR34, Cambridge University, Cambridge, United Kingdom, 1977.
45. M.F. Ashby, C. Gandhi, and D.M.R. Taplin: *Acta Metall.*, 1979, vol. 27, pp. 699...729.
46. C. Gandhi and M.F. Ashby: *Acta Metall.*, 1979, vol. 27, pp. 1565...602.
47. R.J. Fields, T. Weerasooriya, and M.F. Ashby: *Metall. Trans. A*, 1980, vol. 11A, pp. 333...47.
48. A.S. Argon: *Acta Metall.*, 1979, vol. 24, pp. 47...58.